

Climate response to smoke from the burning oil wells in Kuwait

S. Bakan*, A. Chlond*, U. Cubasch*, J. Feichter†, H. Graf*, H. Grassl†, K. Hasselmann*§, I. Kirchner*, M. Latif*, E. Roeckner*, R. Sausen†, U. Schlese*, D. Schriever*, I. Schult*, U. Schumann‡, F. Sielmann† & W. Welke*

* Max-Planck-Institut für Meteorologie, Bundesstrasse 55, D-2000 Hamburg 13, Germany

† Meteorologisches Institut der Universität, Bundesstrasse 55, D-2000 Hamburg 13, Germany

‡ Deutsche Forschungsanstalt für Luft- und Raumfahrt, Institut für Physik der Atmosphäre, D-8031 Oberpfaffenhofen, Germany

The response of the global climate system to smoke from burning oil wells in Kuwait is investigated in a series of numerical experiments using a coupled atmosphere–ocean general circulation model with an interactive soot transport model and extended radiation scheme. The results show a decrease in surface air temperature of $\sim 4^\circ\text{C}$ in the Gulf region. Outside this region the changes are small and statistically insignificant. No weakening of the Indian summer monsoon is observed.

THE question of whether the smoke from the burning oil wells in Kuwait presents a serious threat to global climate has been the subject of considerable scientific debate and widespread public concern. Open oil burning produces a large quantity of soot particles, which absorb sunlight. This leads to a heating of the atmosphere in the absorbing soot layers and a reduction of the solar heating of the Earth's surface. It has been speculated¹ that this modification of the Earth's radiation balance could change the global climate, weakening the Indian monsoon and adversely affecting other climatically sensitive regions.

The effects of soot on the Earth's radiation budget have been much studied in nuclear winter models². The present problem differs in several important aspects from these case studies. In particular, the magnitude and location of the pollution and the height of injection into the atmosphere are reasonably well known and can be expected to have a smaller impact on climate³ than the more extreme nuclear winter scenarios. The climate effects of emissions other than soot are probably negligible. The increase in carbon dioxide emissions, for example, relative to the existing emission level due to global fossil fuel use, is at most a few percent (Kuwait's pre-war contribution to world oil production⁴ was 2.6%).

Our study is restricted to the climate impact of smoke from burning wells on the global scale. Regional climate changes cannot be studied in detail with the relatively coarse resolution ($\sim 5^\circ$) of the available global models. Other environmental questions, such as the influence on stratospheric ozone or other trace gases, and in particular the impact on the ecology, are also not considered.

The model

The model set-up is an extension of the Hamburg global coupled ocean–atmosphere general circulation model which has recently been used in a number of simulations of greenhouse warming^{5,6}. The atmospheric component⁷ is a low-resolution version of the forecast model of the European Centre for Medium-Range Weather Forecasting which has been extensively modified for climate applications (for example, through the inclusion of

liquid water as a prognostic variable⁸). The model uses a dual spectral/grid representation with a triangular truncation at wavenumber 21 (5.6° horizontal resolution), has 19 vertical levels and includes the diurnal cycle and standard physics, such as cloud–radiation interactions⁸. It has been extensively validated and applied in climate studies^{9–11}. The ocean component is the 11-layer Hamburg 'large-scale geostrophic' circulation model, with a horizontal resolution matched to the atmospheric model. This has also been extensively validated and applied in a number of climate experiments^{12–14} and provides the core for the Hamburg–Scripps model of the ocean carbon cycle^{15–17}.

To compensate for the unavoidable initial climate drift of the coupled model, a standard flux correction¹⁸ is applied. This is equivalent to coupling only the deviations from the (not completely matched) initial equilibrium states of the individual subsystems and has no impact on the computed response for small climate perturbations.

The soot distribution is computed with an additional interactive tracer module¹⁹. This includes the processes of advection by the instantaneous three-dimensional velocity field, diffusion, vertical exchange through convection, washout by rain and dry deposition at the surface (assuming a deposition velocity of 0.1 cm s^{-1}). The wet removal rate is a nonlinear function of the local precipitation rate²⁰, which was originally tuned to yield a lifetime of 10 days for highly soluble aerosols (^{210}Pb and ^7Be). As the solubility of soot produced by uncontrolled oil burning, which is strongly contaminated by other substances, is not well known, the relation was returned, in keeping with the worst-case philosophy adopted in this study, to yield a residence time of

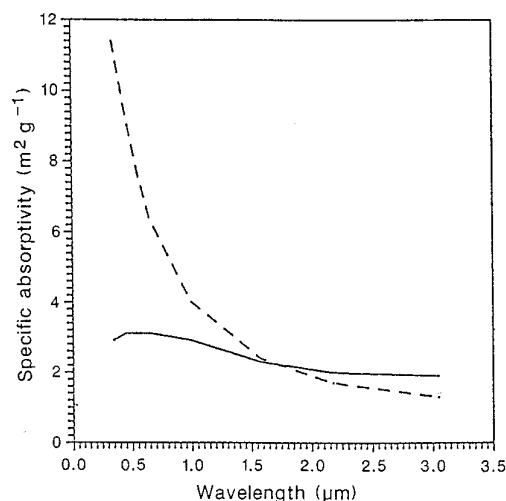


FIG. 1 Specific absorptivities of soot particles ($\text{m}^2\text{ g}^{-1}$) as function of wavelength for two different radius scales for zero-order log-normal particle distributions. Dashed line, $r_m = 0.02\ \mu\text{m}$; solid line, $r_m = 0.1\ \mu\text{m}$. The value of $0.02\ \mu\text{m}$ (radius at the peak of the distribution) was used in the standard scenario.

§ To whom correspondence should be addressed.

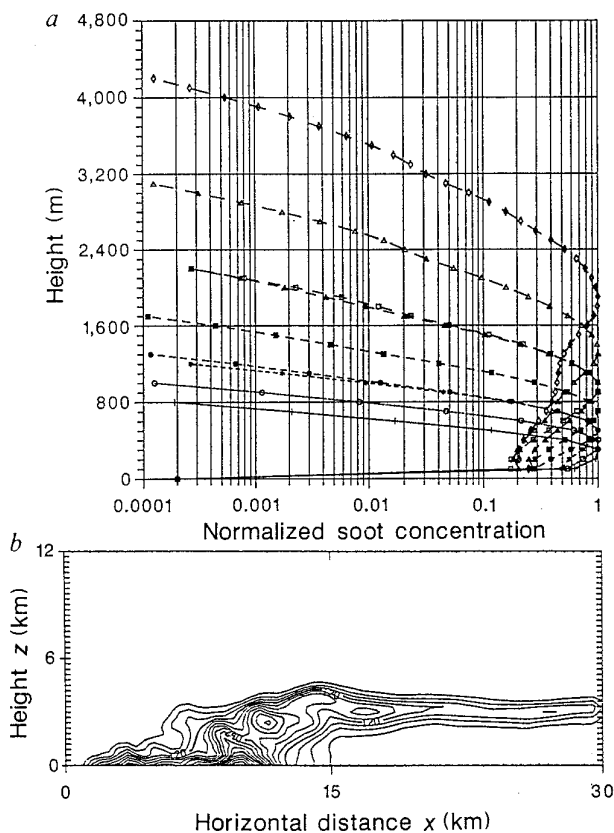


FIG. 2 Estimate of the injection height of the soot using mesoscale circulation models. *a*, Soot profiles for different energy densities, E , and different static stabilities, σ , in the simulation with the first model²³. Runs 1 (+---+---+), 2 (—○—○—○—) and 3 (—*—*—*—), $E=5 \times 10^8 \text{ J s}^{-1}$; runs 4 (—●—●—●—), 5 (—■—■—■—) and 6 (—▲—▲—▲—), $E=2 \times 10^9 \text{ J s}^{-1}$; runs 7 (—□—□—□—), 8 (—△—△—△—) and 9 (—◇—◇—◇—), $E=8 \times 10^9 \text{ J s}^{-1}$. Runs 1, 4 and 7, $\sigma=2.7 \times 10^{-3} \text{ K m}^{-1}$; runs 2, 5 and 8, $\sigma=1.3 \times 10^{-3} \text{ K m}^{-1}$; runs 3, 6 and 9, $\sigma=6.7 \times 10^{-4} \text{ K m}^{-1}$. The energy was released in an area of 4 km^2 . The profiles are normalized by the maximum concentrations. *b*, Height section of the soot concentration in the simulation with the second model²⁴. The contour interval is 0.3 mg per kg .

20 days. All meteorological fields occurring in the computations of soot transport and removal are determined at each point and time by the atmospheric model.

We calculated the feedback of the soot distribution on the model's radiation balance using an extended radiation code based on Mie scattering theory for a size-dependent distribution of (spherical) aerosol particles^{21,22}. The computations are limited to the solar radiation fluxes, as the changes in the thermal infrared radiation were found to be negligible. Although soot particles are not spherical, so that Mie scattering theory is not strictly applicable, the computed net absorption coefficient ($\sim 8 \text{ m}^2 \text{ g}^{-1}$) for the size distribution assumed in the standard scheme (a zero-order log normal distribution with a mode radius²³ of $0.02 \mu\text{m}$) is in order-of-magnitude agreement with measurements (ref. 2 and Fig. 1). The effect of soot particles on clouds, through the increase in cloud condensation nuclei or through the enhanced absorption of radiation by cloud droplets containing soot particles²⁴ could not be investigated with the present model.

The worst-case scenario

A number of climate simulations were carried out, but we shall present results only for the standard (worst-case) scenario. In this experiment, a constant burning rate of 440,000 tonnes oil per day (~ 3.1 million barrels per day) is assumed, corresponding to twice the pre-war production of Kuwait⁴. This is less than

the considerably higher burning rates frequently quoted by Kuwait sources, but about 50% higher than calculations based on Kuwait oil-well data and estimates of reservoir pressure³. The burning is assumed to begin on 15 February and continue until the following January. The model was initialized by a 100-year integration (which had been made as a control run for other experiments addressing greenhouse warming⁵).

We assume that 10% of the oil (mass ratio) is converted to soot². This represents a reasonable mean value of experimental data for burning oil pools, but is probably rather high for better-ventilated burning oil wells. The soot is introduced into the atmosphere at a single model gridpoint, but some spatial smoothing is applied to avoid negative concentrations arising from the numerical truncation of the spectral model. To allow for the rapid sedimentation of large soot particles within the first 500-km grid cell, the source strength is reduced by 15%, so that the net effective soot injection rate on the model scale is 37,400 tonnes per day.

The soot is injected initially at a constant mixing ratio into the lowest two kilometres of the atmosphere (more precisely, into model levels 2–5, between 60 m and 1,800 m). The initial injection profile is based on mesoscale simulations of 'nuclear winter'²⁵, on our own computations using two different three-dimensional, nonhydrostatic mesoscale models and on satellite observations. If all the oil is assumed to be burned in an area of $20 \times 20 \text{ km}^2$, the energy release, assuming a typical energy equivalent for oil of $4 \times 10^4 \text{ J kg}^{-1}$, yields a heat flux of 500 W m^{-2} . According to the mesoscale model simulations for nuclear winter²⁵, this results in injection heights, depending on the atmospheric stability, of about 2 km. Figure 2a shows the corresponding injection heights computed with one of our mesoscale models²⁶ for various values of the atmospheric static stability and surface heat release. These curves, as well as the results of a second mesoscale model²⁷ (Fig. 2b shows an example of a soot plume computed with this model) indicate that for the range of static stabilities typical of the Gulf region, in which unstable deep cumulus convection events are rare, the soot injection will normally not exceed a height of 2–4 km, even for the relatively large heat fluxes assumed in our simulations. This is supported, finally, by an analysis²⁸ of a satellite observation of the soot cloud over Kuwait on 24 February 1991, which indicated that the cloud did not exceed a height of 3 km.

The relatively low injection height is an important factor in limiting the global climate impact of the soot release³. The soot is transported in atmospheric layers in which it can be rather rapidly washed out and removed by dry deposition. The 20-day residence time of soot in the troposphere is small compared with typical residence times of aerosol in the stratosphere, which are several years. Also, the opposing effects of atmospheric heating in the absorbing soot layers and cooling of the Earth's surface can be more easily compensated in the lower troposphere through vertical energy transfer.

The soot distribution becomes quasi-stationary one or two months after the oil burning begins on 15 February. The total

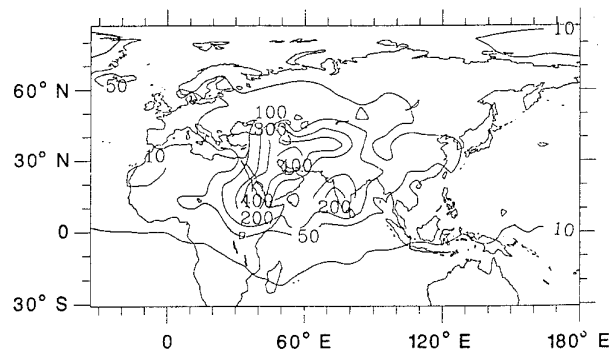


FIG. 3 Total deposition of soot (mg m^{-2}) during the 12-month simulation. Contour intervals are at 10, 50, 100, 200, 300 and 400 mg m^{-2} .

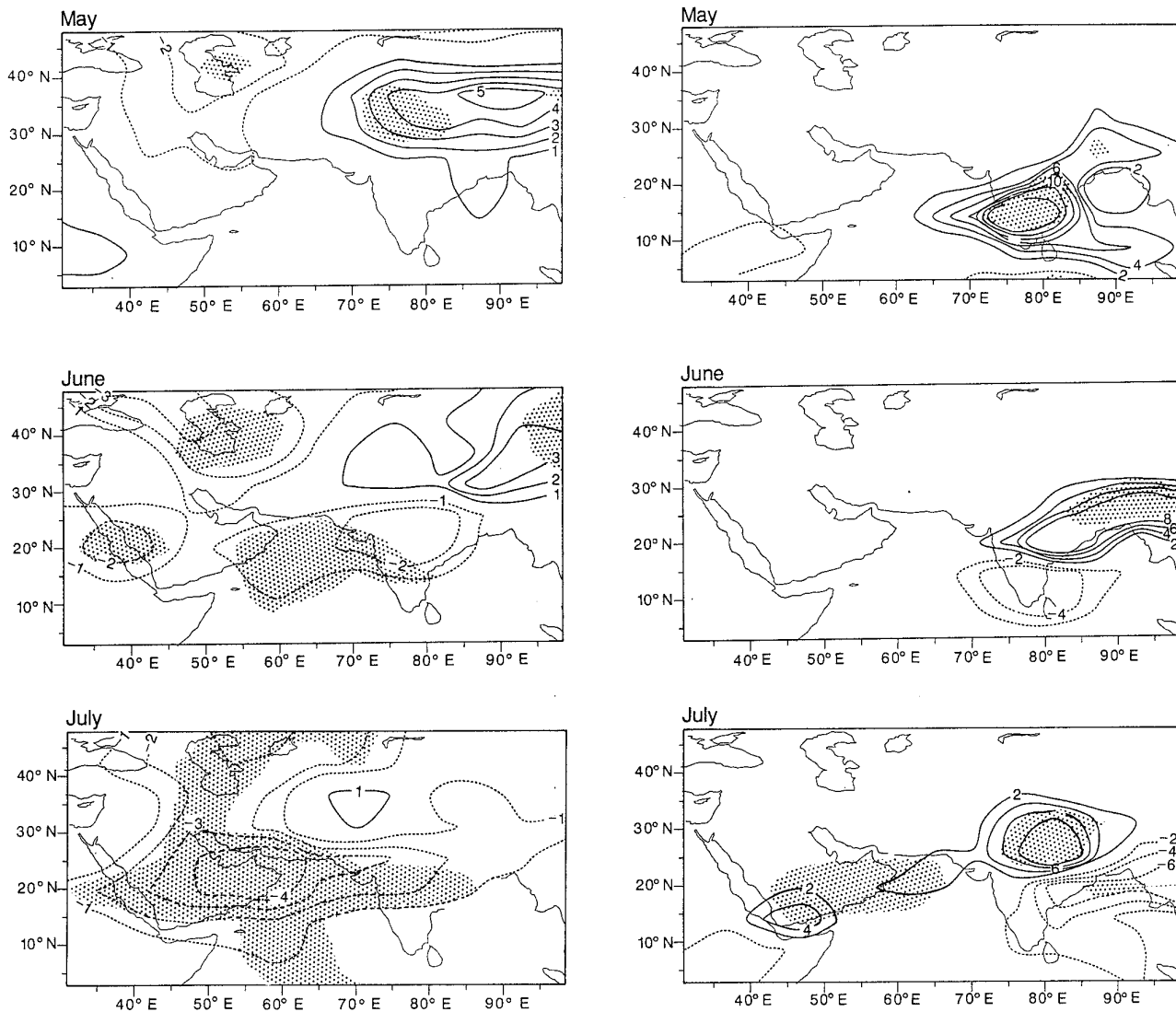


FIG. 4 Climate response in summer. Left: anomalous 2-m temperature. Contour interval is 1 °C. Right: Anomalous precipitation. Contour interval is

2 mm per day. The zero contours have been suppressed. Shading indicates regions with local significance levels larger than 95%.

atmospheric soot content in the quasi-stationary state is $\sim 7 \times 10^8$ kg. The soot does not rise significantly higher than three kilometres. The highest altitudes are attained in the summer, when the increased solar radiation increases the convective activity. The self-lofting of the soot (the buoyancy uplift caused by the absorption of solar radiation in the layers of a high soot concentration) is also largest in the summer. But numerical experiments with a mesoscale model²⁶ indicate that this effect is small compared with the turbulent mixing. The transport of soot into the stratosphere is negligible: $\sim 0.3\%$ (2,100 tons) of the total atmospheric soot load is found in the stratosphere.

Most of the soot is deposited, primarily through wash-out by rain, within a few thousand kilometres from the source (Fig. 3). The maximum surface densities of ~ 400 mg m⁻² after one year of continual burning are found in Iran (the assumed deposition of 15% of the soot emission in the immediate vicinity of the oil wells, which can yield densities two to three orders of magnitude larger than this value, is not shown in Fig. 3).

The climate response to the atmospheric soot loading was determined as the difference between the worst-case scenario and the control run. As expected from Fig. 3, considerable anomalies in the radiation field are found only on regional scales within a few thousand kilometres from the source. The reduction off the net solar radiation reaching the Earth's surface in this

region is $\sim 20\%$, while the net absorbed solar radiation by the atmosphere and Earth's surface is increased by 15%. The total optical depth of the cloud, including absorption and scattering, is ~ 0.4 .

The surface deposition of soot also affects the surface albedo, in particular for snow-covered surfaces. Soot that is covered by fresh snowfall in the winter reappears during the melting period, when the accumulated soot concentration can increase to values of 10 p.p.m. This can reduce the albedo of the snow from 60% to $\sim 40\%$ (ref. 29). The area of polluted snow is small, however, and the duration of the melting period is short. On the basis of previous sensitivity experiments¹¹ with changed snow covers, we regarded the albedo effect as negligible and did not include it in the radiation computations.

It is well known from El Niño/Southern Oscillation (ENSO) studies¹⁰ and other atmospheric response experiments that regional-scale heat flux or radiation anomalies can generate global-scale atmospheric anomalies. But there is no obvious large-scale structure evident in either the temperature or the precipitation fields that is distinguishable from the inherent model interannual variability (r.m.s. monthly mean deviations of ~ 2 °C in temperature and 50%, but very small scale, in precipitation^{5,8}). On the regional scale, significant temperature anomalies are seen mainly near the source region (Fig. 4, left),

with a maximum cooling of $\sim 4^\circ\text{C}$ in July. All values shown represent averages over at least a model grid square of side 500 km and a period of one month. The temperature decrease can be much stronger in smaller regions and timescales below dense smoke plumes. Outside the Gulf region, considerable anomalous heating is found over the Tibetan Plateau in May. This is probably due to the proximity of the absorbing soot layers in the atmosphere to the surface at these high altitudes (after May, the soot trajectories move further south).

In the precipitation distributions (Fig. 4, right), there is no indication of a weakening of the Indian summer monsoon, as has frequently been speculated. There is even a region of enhanced rainfall over India during the onset phase of the monsoon in May, in response to the anomalous heating over Tibet. The enhanced rainfall region shifts further north during the following two months.

The conclusion that, on the global scale, the anomaly fields cannot be distinguished from the natural model variability is supported by a lack of agreement between the global response patterns found in the standard scheme and a number of further sensitivity runs made with modified input and model parameters.

Sensitivity studies

To investigate the dependence of the simulation results on some of the more critical input and model assumptions, we carried out a series of additional experiments. First, the value for soot emission was changed. Halving the emission roughly halved the amplitude of the climate response in the near-field regions, whereas the large-scale response was again indistinguishable from noise. But an alternative scheme, in which a number of input parameters were changed simultaneously to yield an effective increase of the emissions by an (unrealistic) factor of 4, produced a considerable climate response on the global scale, with temperature decreases, and in some regions increases, of about $5\text{--}10^\circ\text{C}$. Interpolating between the three simulations, we conclude that although the large-scale climate change in the worst-case scenario is smaller than the natural interannual variability, it is not far from the detectability threshold.

Because of the large uncertainty in the size and the resultant specific absorption of soot particles, we considered an alternative size distribution of soot particles. The particle distribution was rescaled to a mode radius of $0.1\ \mu\text{m}$ instead of $0.02\ \mu\text{m}$, yielding a reduction of the specific absorption cross-section by a factor 2–4 in the relevant solar spectral band (Fig. 1). The near-field climate response decreased by a similar factor and was barely detectable above the natural variability. The true size distribution presumably lies somewhere between these cases², but because of the flakelike geometry of soot particles the first scenario is probably more realistic.

Further sensitivity experiments were carried out with modified injection heights and larger washout rates corresponding to residence times of about 10 days. The sensitivity with respect to these parameters was approximately linear. In summary, our standard model may be regarded as a reasonable worst-case scenario within the range of uncertainties of the various input and model parameters.

Discussion

An advantage of the fully coupled model system used in this study is that all processes are computed interactively. Thus the effect on the soot transport of the thermal uplift induced by warming in the layers of maximal soot concentration is automatically included, as is the inhibition of the vertical transport of soot because of the higher static stability established between the heated layers and the cooled surface. Similarly, the complete feedback chain describing the influence of the changed circulation on the precipitation distribution and thus on the soot washout rate, and thereby, finally, on the radiation perturbations driving the circulation change, is incorporated into a single model.

The oceans, although also coupled fully interactively with the atmosphere, play a relatively small part in the present experi-

ment. The deep ocean circulation does not change significantly in the short one-year integration period, and the changes in the more rapidly responding upper layers and in the sea ice distribution occur in regions where the climate changes cannot be detected above the natural variability background.

The principal reason for the lack of a statistically significant global climate response outside the near-source region is the relatively low initial height for soot injection. This in turn is governed by the limited heat release and the finite static atmospheric stability. The low injection level enables the soot to be washed out or removed by dry deposition in a typical lifetime of 20 days. Only 0.3% is transported into the stratosphere, where soot can survive for several years.

The limited height of the soot distribution also enables the positive and negative anomalies in the radiation balance induced by the smoke to be more easily compensated through the turbulent energy exchange and infrared radiation fluxes in the lower troposphere: the increased downward longwave radiation from the layers of high soot concentration, which are warmed by the absorption of solar radiation, and the decreased upward turbulent heat fluxes from the surface, which is cooled by the reduced solar flux below the smoke cloud, counteract these opposing temperature trends.

Although we were unable to detect a statistically significant climate signal on the global scale in our one-year standard scenario (or any of the other sensitivity experiments, apart from the unrealistic case in which the effective soot emissions were increased by a factor of four), this does not imply that such a signal cannot be found. By extending the experiment over a number of years, or carrying out an ensemble of such experiments, the persistent response pattern could presumably have been filtered out from the nonrecurrent natural interannual variability. But the fact that the signal could not be detected in a one-year integration implies that the global climate perturbation should have little impact in practice.

The large global climate response obtained when the effective soot emission was increased by a factor of four indicates, however, that our standard scenario could not have been very far from the detectability threshold, even for a one-year simulation, and may serve as a timely reminder that our global climate is indeed vulnerable to irresponsible actions by man. \square

1. Aldhus, P. *Nature* **349**, 96 (1991).
2. Pittcock, A. B. *et al. Scope* **28**, 1 (1986).
3. Small, R. D. *Nature* **360**, 11–12 (1991).
4. *Statistical Review of World Energy* (British Petroleum Company, London, 1990).
5. Cubasch, U., Sausen, R., Oberhuber, J., Lunkeit, F. & Böttinger, M. Simulation of the greenhouse effect with coupled ocean-atmosphere models *Cray Channels* **12**, 6–9 (1990).
6. Hasselmann, K. *Tellus* (in the press).
7. Dürnenil, L. & Schlese, U. *Meteor. Inst. Univ. Hamburg, Rep. No. 1* (Hamburg, 1987).
8. Roeckner, E. *et al. WMO/TD No. 322* (WMO, Geneva, 1989).
9. Cess, R. D. *et al. Science* **245**, 513–516 (1989).
10. Latif, M., Biercamp, J., v. Storch, H., McPhaden, M. J. & Kirk, E. *J. Clim.* **3**, 509–521 (1990).
11. Barnett, T. P., Dürnenil, L., Schlese, U., Roeckner, E. & Latif, M. *J. Atmos. Sci.* **46**, 661–685 (1989).
12. U. Mikolajewicz, Santer, B. D. & Maier-Reimer, E. *Nature* **345**, 589–593 (1990).
13. U. Mikolajewicz & Maier-Reimer, E. *Clim. Dynam.* **4**, 145–156 (1990).
14. Maier-Reimer, E. & Mikolajewicz, U. *Experiments with an OGCM on the Cause of the Younger Dryas, Oceanography 1988* (eds Ayala-Castanares, A., Wooster, W. & Yanez-Arancibia, A.) 87–100 (UNAM Press, Mexico City, 1989).
15. Maier-Reimer, E. & Hasselmann, K. *Clim. Dynam.* **2**, 63–90 (1987).
16. Heinze, C., Maier-Reimer, E. & Winn, K. *Palaeoceanography* (in the press).
17. Bacastow, R. & Maier-Reimer, E. *Clim. Dynam.* **4**, 95–125.
18. Sausen, R., Barthel, K. & Hasselmann, K. *Clim. Dynam.* **2**, 145–163 (1988).
19. Feichter, J., Roeckner, E., Schlese, U. & Windelband, M. *Proc. 18th ITM on air pollution modelling and its applications* (ed. Van Dop, H.) (Plenum, New York, in the press).
20. Giorgio, F. & Chameides, W. L. *J. geophys. Res.* **91**, 14367–14376 (1986).
21. Bakan, S. thesis, Univ. Hamburg (1982).
22. Schult, I. thesis, Max-Planck-Inst. Meteorol., Hamburg (1991).
23. Espenscheid, W. F., Kerker, M. & Matijevic, E. *J. phys. Chem.* **68**, 3093–3097 (1964).
24. Grassl, H. *The Changing Atmosphere, Dahlem Workshop Reports* (eds Rowland, F. S. & Isaksen, I. J. A.) 187–199 (Wiley, Chichester, 1988).
25. Penner, J. E., Haselman, L. C. & Edwards, L. L. *J. Clim. appl. Met.* **25**, 1434–1444 (1986).
26. Chlond, A. *Boundary-Layer Meteorol.* (submitted).
27. Schumann, U., Hauf, T., Höller, H., Schnidt, H. & Volkert, H. *Beitr. Phys. Atmos.* **60**, 413–446 (1987).
28. Schumann, U. *DLR preliminary rep.* (DLR, Oberpfaffenhofen, 1991).
29. Warren, S. G. & Wiscombe, W. J. *J. Atmos. Sci.* **37**, 2734–2745 (1980).

ACKNOWLEDGEMENTS. This research was mainly supported by the Bundesministerium für Forschung und Technologie (BMFT). The computations were carried out at the Deutsches Klimarechenzentrum, which is supported by the BMFT, the Max-Planck-Gesellschaft, the Freie und Hansestadt Hamburg, the Alfred Wegener Institut für Polar- und Meeresforschung and the Forschungszentrum Geesthacht. We are grateful to M. Grunert for preparing the diagrams.